V Michaud-Belleau, H Bergeron, P S Light, N B Hébert, J D Deschênes, A N Luiten and J Genest

Passive coherent discriminator using phase diversity for the simultaneous measurement of frequency noise and intensity noise of a continuous-wave laser

Passive coherent discriminator using phase diversity for the simultaneous measurement of frequency noise and intensity noise of a continuous-wave laser

V Michaud-Belleau[1]**, H Bergeron**[1]**, P S Light**[2]**, N B Hébert**[1]**, J D Deschênes**[1]**, A N Luiten**[2] **and J Genest**[1]

[1] Centre d'optique, photonique et laser, Université Laval, Québec, QC, G1V 0A6, Canada
[2] Institute for Photonics and Advanced Sensing and School of Physical Sciences, University of Adelaide, Adelaide, SA 5005, Australia

E-mail: `jerome.genest@gel.ulaval.ca`

Abstract. The frequency noise and intensity noise of a laser set the performance limits in many modern photonics applications and, consequently, must often be characterized. As lasers continue to improve, the measurement of these noises however becomes increasingly challenging. Current approaches for the characterization of very high-performance lasers often call for a second laser with equal or higher performance to the one that is to be measured, an incoherent interferometer having an extremely long delay-arm, or an interferometer that relies on an active device. These instrumental features can be impractical or problematic under certain experimental conditions. As an alternative, this paper presents an entirely passive coherent interferometer that employs an optical 90° hybrid coupler to perform in-phase and quadrature detection. We demonstrate the technique by measuring the frequency noise power spectral density of a highly-stable 192 THz (1560 nm) fiber laser over five frequency decades. Simultaneously, we are able to measure its relative intensity noise power spectral density and characterize the correlation between its amplitude noise and phase noise. We correct some common misconceptions through a detailed theoretical analysis and demonstrate the necessity to account for normal imperfections of the optical 90° hybrid coupler. We finally conclude that this passive coherent discriminator is suitable for reliable and simple noise characterization of highly-stable lasers, with bandwidth and dynamic range benefits but susceptibility to additive noise contamination.

1. Introduction

A key characteristic distinguishing lasers from standard light sources is their intrinsically high temporal coherence, or slowly decaying electric field autocorrelation function, the Fourier equivalent of a narrow lineshape [1]. The need for a high degree of temporal coherence arises in important applications such as frequency metrology [2], coherent optical communications [3], and spectroscopy [4]. For these applications, one often needs to perform a quantitative measurement of the degree of temporal coherence of a continuous-wave (CW) laser. This is usually stated through a measurement of its Allan deviation (conventionally at long timescales), its spectral lineshape, or its frequency and intensity noise properties (conventionally at short timescales) [5]. These two last measurements contain the maximum information available and can be used to derive both the lineshape and Allan deviation if required (only phase or frequency noise is required in the latter case) [6, 7].

Historically, as progress in laser technology brought the linewidth of lasers below a single gigahertz, common characterization techniques using scanning filters or parallel filter banks (Fabry-Perot cavity, diffraction grating, etc.) became obsolete because of their insufficient frequency resolution; standard radio-frequency (RF) characterization techniques were then transposed to the optical domain [8]. Today, with state-of-the-art lasers having linewidths below a single hertz [9] and most commercial lasers having linewidths below 100 MHz, these RF characterization techniques are ubiquitous. The underlying idea of these techniques is to use a high-performance optical local oscillator (LO), which is typically a laser, and a photodetector to downconvert the optical field of the laser under test into the electrical domain where its, Allan deviation, lineshape, or frequency and intensity noise properties are more easily measured.

The origin of the LO, whose temporal coherence also contributes to the measurement, is usually the main distinction between different techniques. When a second laser that is more frequency-stable than the laser under test is available to act as the LO, the so-called heterodyne approach is often preferred [10, 11]. However, the LO can also be conveniently generated from the laser under test using a delay-line interferometer that combines the laser field with a delayed and possibly frequency-shifted version of itself,

therefore avoiding the use of a reference laser. In this case, the phase noise of the delay-line acts as the measurement floor for phase measurements, replacing in this role the LO phase noise of the heterodyne approach. If the delay is such that the recombined fields are decorrelated for all timescales of interest, the method is then called "incoherent" and is in essence equivalent to the heterodyne method using two independent but otherwise identical lasers [12]. For the characterization of highly-stable lasers, the challenge is that multi-kilometer delay-lines become necessary to achieve such decorrelation. This comes with many practical limitations that are detailed in the appendix. A more convenient approach in this case is to use a coherent interferometer (i.e., that introduces a delay much shorter than the coherence time of the laser under test) and then take the correlation between the combined fields into account when processing the extracted signals [13, 14]. Such an interferometer is often called a "coherent discriminator", "frequency discriminator", or "delay-line discriminator", in analogy with frequency-modulation detection circuits for RF and microwave applications [15], or simply a "coherent homodyne interferometer". The present paper focuses on this high-correlation regime since it provides the best signal-to-noise ratio (SNR) between laser noise and delay-line noise as further explained in the appendix.

The most basic implementation of the coherent discrimator is fully passive. A typical instrument can take the form of a fiber Mach-Zehnder interferometer [16] [figure 1(a)] or Michelson interferometer [17], although multiple-beam interferometer configurations have also been demonstrated [18, 19]. The underlying principle remains the same in all cases: when the differential delay is such that the interferometer output is held at the side of an interference fringe, halfway between the maximum and minimum output values, the instrument effectively converts phase or frequency fluctuations into intensity fluctuations that can be readily measured with standard photodetectors. Without loss of generality, we will concentrate on the fiber version of the Mach-Zehnder interferometer in this paper.

Even though the coherent discriminator has been used for decades, it has limitations that sometimes lead to inaccurate or impractical measurements. These problems have often been overcome by adding an active modulation device in one arm of the interferometer, a modification that is not always desirable. The

technique we describe and demonstrate here does not require any active modulation device and still overcomes the known limitations of the coherent discriminator, with dynamic range and bandwidth benefits. This is achieved by replacing the 50/50 output coupler of the interferometer with an optical 90° hybrid coupler in order to perform in-phase (I) and quadrature (Q) detection of the mixed optical fields [figure 1(b)]. This is commonly done in the field of optical communications [20, 21, 22]. However, this idea has not yet significantly diffused to the optical metrology community and has not been applied for the characterization of highly-stable lasers. The remainder of the paper details this idea and is organized as follows: we start with a description of the basic coherent discriminator that serves as baseline for the ensuing theoretical analysis; possible improvements are then progressively introduced to bring us to the proposed design. While this analysis relies on well-known concepts, it helps correcting misconceptions that frequently appear in the literature and gives a firm basis for identifying the advantages and disadvantages of the instrument with respect to other known approaches. We finish with an experimental demonstration showing that this instrument is suitable for the characterization of highly-stable lasers.

2. General theory

2.1. Description of the basic configuration

We start by defining the incident electric field in figure 1(a) through its real representation,

$$E(t) = E_0[1 + \epsilon(t)] \cos[2\pi\nu_0 t + \phi(t) + \phi_0], \quad (1)$$

where E_0 is the average field amplitude, $\epsilon(t)$ represents relative amplitude noise that can be related to relative intensity noise through squaring, $\phi(t)$ represents the instantaneous phase fluctuations that can be related to frequency noise through differentiation, ν_0 represents the carrier frequency, and ϕ_0 is an initial phase. Following [23], we assume that both $\epsilon(t)$ and $\phi(t)$ are zero-mean wide-sense stationary random processes that are mean-square continuous.

The incident field is split by the input coupler and recombined at the output coupler after the introduction of a differential delay T. Although the interferometer output is often maintained at the side of a fringe for maximum phase noise conversion, the more general case of an arbitrary fringe position will be considered first. A standard treatment [17], valid for the Michelson or the Mach-Zehnder interferometer with perfect 50/50 coupling and polarization management, leads to the approximate photocurrent at one of the two output
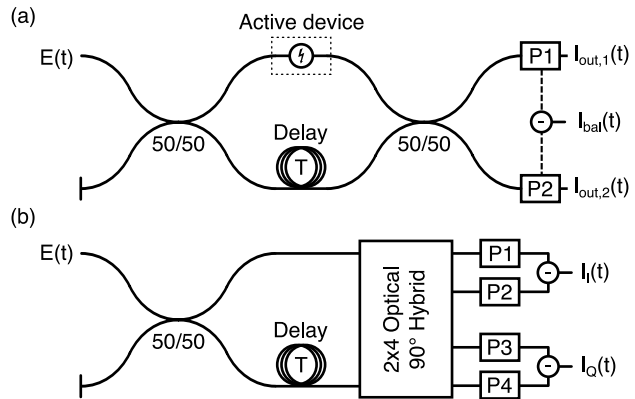

Figure 1. (a) Typical configuration of a fiber delay interferometer. When present, the active device is often an EOM, AOM, or fiber stretcher. (b) Passive configuration described in this paper. Note that polarization-maintaining components are used extensively and that P1 to P4 represent photodiodes.

ports,

$$I_{\text{out},1,2}(t) \approx \frac{RP_0}{2}[1 + \epsilon(t) + \epsilon(t - T)]$$
$$\times \{1 \mp \cos[\phi(t) - \phi(t - T) + 2\pi\nu_0 T]\}, \quad (2)$$

where R is the detector responsivity, $P_0 = E_0^2 S/(2\eta)$ is the average incident power on a surface of area S, and η is the impedance of the medium where the electric field is computed. The sign choice in the equation above is determined by which output port is being examined. To obtain this last equation, two additional assumptions are made: first, the relative amplitude fluctuations $\epsilon(t)$ are assumed much smaller than 1 so terms of the form $\epsilon^2(t)$ are neglected. This is true for most CW lasers [1]. Second, the effect of having unequal dispersion and absorption in the two interferometer arms is neglected and it is assumed that the optical power is low enough so as to avoid any optical nonlinear effect in the fiber.

The differential phase noise $\phi(t) - \phi(t - T)$ is usually the quantity of interest as it can be processed to extract laser phase noise or frequency noise information. This quantity is however inseparable from $2\pi\nu_0 T$, a variable that we will call "fringe phase" throughout this paper. In this context, it is therefore important for the fringe phase to be stable, or in other words for the fringe phase noise (interferometer) to be lower than the differential phase noise (laser) for all timescales of interest, assuming that any noise on the laser carrier frequency is lumped in the laser phase noise term. Unless it is explicitly mentioned, we will consider a perfectly constant fringe phase in the following theoretical development. Since the differential phase noise appears inside a cosine function, it generally cannot be extracted directly and unambiguously. A simple way to avoid this problem

is to make the delay such that the standard deviation of the differential phase noise is much less than one radian. This necessarily follows from the correlation of the combined electric fields in the coherent regime and it enables the linearization of the cosine function (small angle approximation, more accurate at the side of a fringe), which physically means that the interferometer's output signal can be considered locally linear at any fringe point if the laser phase variation in a time T is sufficiently small. This linearization yields a less general expression for the photocurrent:

$$I_{\text{out},1,2}(t) \approx \frac{RP_0}{2}\{[1 + \epsilon(t) + \epsilon(t - T)][1 \mp \cos(2\pi\nu_0 T)]$$
$$\pm [\phi(t) - \phi(t - T)]\sin(2\pi\nu_0 T)\}. \qquad (3)$$

As can be recognized from (3), the photocurrent contains a constant that is the average or deterministic output of a two-port interferometer, $RP_0[1 \mp \cos(2\pi\nu_0 T)]/2$, where the value of $2\pi\nu_0 T$ determines whether constructive, destructive or partial interference is observed on average at the chosen output. The photocurrent also contains filtered amplitude noise and filtered phase noise (i.e., sum of delayed terms and difference of delayed terms, respectively) that are added to the average output in a proportion that depends on the fringe phase. This filtering action together with the fringe phase determine the properties of the output signal. Using only the second output port in figure 1(a), we obtain useful insight into the behavior of the instrument by computing the Fourier transform of the AC autocorrelation function of the photocurrent with respect to its average value. This gives the expression for the double-sided normalized photocurrent power spectral density (PSD) $\widehat{S_I}(f)$, valid for any fringe phase $2\pi\nu_0 T$, but only for small differential phase $\phi(t) - \phi(t - T)$ and thus only valid for coherent operation:

$$\widehat{S_I}(f) \approx (2\pi T)^2 \sin^2(2\pi\nu_0 T)\text{sinc}^2(fT)S_\nu(f)$$
$$+ 4\cos^4(\pi\nu_0 T)\cos^2(\pi fT)S_{\text{RIN}}(f) \qquad (4)$$
$$- 8\cos^2(\pi\nu_0 T)\sin(2\pi\nu_0 T)\sin(2\pi fT)$$
$$\times \text{Im}[S_{\epsilon,\phi}(f)],$$

where f is the Fourier frequency, $S_\nu(f)$ is the frequency noise (FN) PSD, $S_{\text{RIN}}(f)$ is the relative intensity noise (RIN) PSD, $S_{\epsilon,\phi}(f)$ is the cross-PSD between phase noise and amplitude noise and $\text{sinc}(x)$ is the normalized cardinal sine function. The relations $I_0 \equiv RP_0/2$, $\widehat{S_I}(f) \equiv S_I(f)/I_0^2$, $S_\nu(f) = f^2 S_\phi(f)$ and $S_{\text{RIN}}(f) \approx 4S_\epsilon(f)$ were used to simplify the last equation. Formally, there is a distinction between the power spectral density, which is a theoretical curve as in the last equation, and the experimental spectrum, often called periodogram, that is used to estimate the PSD. Here, we will call both the theoretical and experimental curves "PSD" for simplicity, the context being sufficient to distinguish each of them.

From the last equation, we note that for phase noise the interferometer introduces a squared sine transfer function (in the sense of power gain as a function of frequency) having a null at DC, but the relationship between phase and frequency turns it into a squared cardinal sine when FN is considered. This FN transfer function has a low-frequency gain of $(2\pi T)^2$ that scales with the delay, therefore allowing the adjustment of the sensitivity of the interferometer, and remains almost constant from DC up to an appreciable fraction of the first null frequency $1/T$ (figure 2). It should be noted that the value of I_0 must be measured in order to properly calibrate the current PSD. The RIN PSD and the amplitude-phase cross-PSD are also filtered by the interferometer. Even though these three filters are sometimes regarded as an inconvenience, much of the relevant laser noise is often located within a limited bandwidth, for example at Fourier frequencies below the laser's relaxation oscillations [24], or simply within a user-defined bandwidth. Therefore, the differential delay T can be coarsely adjusted so that most of the noise of interest is kept within the almost constant section of the three transfer functions where it is possible to divide their spectral shape without worrying about their zeros. Still, a coarse adjustment of this delay solely based on the desired bandwidth may lead to a gain $(2\pi T)^2$ insufficient to pull the signal above the measurement noise floor. In this case, one must increase the delay and accept the loss of bandwidth. Once the value of the differential delay is coarsely adjusted to meet these critera, fine adjustements at the fringe level determine if the interferometer is set for maximum RIN conversion or maximum FN conversion, the latter being the most common condition of operation.

2.2. Problems with the basic configuration and standard solutions

The basic coherent discriminator is a convenient instrument but it has some limitations that will be outlined here along with some common solutions. First, and as indicated before, the efficient conversion from FN to current noise requires the delay to be adjusted and maintained so that the signal sits, on average, at the side of an interference fringe. This is reflected in (3) and (4) where a value of $2\pi\nu_0 T$ that is an odd multiple of $\pi/2$ maximizes FN conversion. This implies that a slow drift of the laser carrier frequency or of the differential delay set by the interferometer limits the available measurement time as the interferometer then cycles between maximum and minimum FN conversion. Therefore, an active device such as an electro-optic modulator (EOM) or a fiber stretcher is often used as the actuator of a servo-loop that locks the interferometer to the laser at low Fourier frequencies
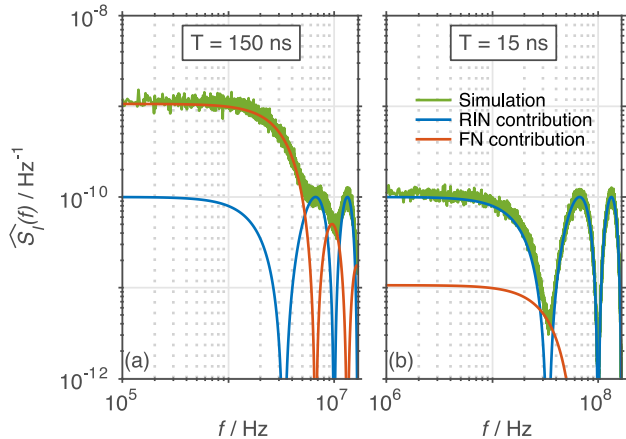
Figure 2. Single-sided (SS) normalized photocurrent PSD of the basic coherent discriminator adjusted for maximum FN conversion. A simulation with a white (flat) SS FN PSD of 1200 Hz^2/Hz and a white SS RIN PSD of 10^{-10} Hz^{-1} is compared to equation (4). Both noises are independent. (a) The delay of 150 ns is sufficient for the FN to dominate in most of the Fourier frequency range. (b) With a shorter delay, it is the RIN that dominates the measurement. The critical delay in this case is constant at 45 ns for all frequencies.

in order to maintain a specific fringe condition [25]. An equivalent solution is to lock the laser frequency to the side of an interference fringe using the laser's actuators [26]. In both cases, computing the FN within the servo bandwidth requires a careful characterization of the loop gain versus frequency.

Examination of (4) shows a second problem with conventional measurements: RIN is converted into current noise even when the interferometer is set for maximum FN conversion ($2\pi\nu_0 T = \pi/2$, figure 2). This effect is often neglected but it clearly sets a frequency-dependent limit on the delay required to guarantee predominance of the FN term in (4). This limit can be expressed as the critical delay for which RIN and FN are equal at a given Fourier frequency, $T_{crit}(f) = [S_{RIN}(f)/S_\nu(f)]^{1/2}/(2\pi)$. Besides setting $T \gg T_{crit}(f)$ for all frequencies of interest, which requires preliminary information about the RIN and FN levels, a standard way to avoid this issue is to use balanced detection [27]; by subtracting the photocurrents measured from the two output ports, the RIN contribution is theoretically canceled, and in practice reduced, when the interferometer is set for maximum FN conversion.

The third technical limitation of the coherent discriminator is that additive noise can contaminate the measurement and be interpreted as real laser noise. This is typically a problem at low frequencies where additive noise PSDs tends to rise. It can usually be avoided by shifting the spectrum using an acousto-optic modulator (AOM) [29]. With balanced detection,

the photocurrent is then

$$I_{\text{bal}}(t) \approx RP_0[1 + \epsilon(t) + \epsilon(t-T)]$$
$$\times \cos[\phi(t) - \phi(t-T) + 2\pi\nu_0 T + 2\pi\Delta ft], \quad (5)$$

where Δf is the positive AOM frequency shift. Provided the amplitude and phase noises are bandlimited, other pre-detection noises are low enough, and the frequency shift is sufficient, the output photocurrent is then a passband signal centered at Δf. This signal, which is most often studied with a spectrum analyzer, has a PSD that is almost identical to (4) but centered at Δf [figure 3(a)]. However, in addition to the increased immunity to low-frequency additive noise, the modulation averages out the fringe phase. Long measurement times are thus allowed without any kind of active stabilization. Still, processing this signal with a scalar spectrum analyzer means that it is no longer possible to completely decouple RIN and FN from the PSD of the photocurrent, even with perfect balancing.

A powerful but uncommon alternative to the spectrum-analyzer-based processing consists in computing the analytic representation of the signal from the digitized passband photocurrent [30]. Indeed, the AOM frequency shift, if sufficient, allows the software extraction or demodulation of the differential phase from the cosine function of (2) and a simultaneous yet independent extraction of the filtered amplitude [figure 3(b-c)]. This is possible without any linearization operation and it is therefore valid for any value of the delay T (coherent or incoherent regime), which simplifies the analysis in the transition between the two regimes. With this method, the filtered FN PSD and the RIN PSD can be obtained separately, without cross-contamination, and still without reliance on maintaining a specific fringe phase. Even though the RIN can be simply measured through direct detection, it can be convenient to access both quantities in a single measurement [16]. Moreover, the amplitude-phase cross-PSD, a quantity that carries useful information [31], is accessible and a separate calibration measurement of I_0 is no longer required to scale the FN PSD. It is however still required to scale the RIN PSD.

Nevertheless, the bandlimited noise condition required to properly compute the analytic representation of the signal can be difficult to meet in certain cases. The modulator can moreover introduce a certain amount of loss, filtering, harmonic distortion, and excess noise [32, 33] and the optical power that it dissipates can cause problems with the thermal stabilization of the interferometer [34, 35]. Its use also results in an increased complexity of the supporting optics and electronics [36]. These features are not problematic in all cases, but they may stimulate the choice of an alternative instrument in some of them.
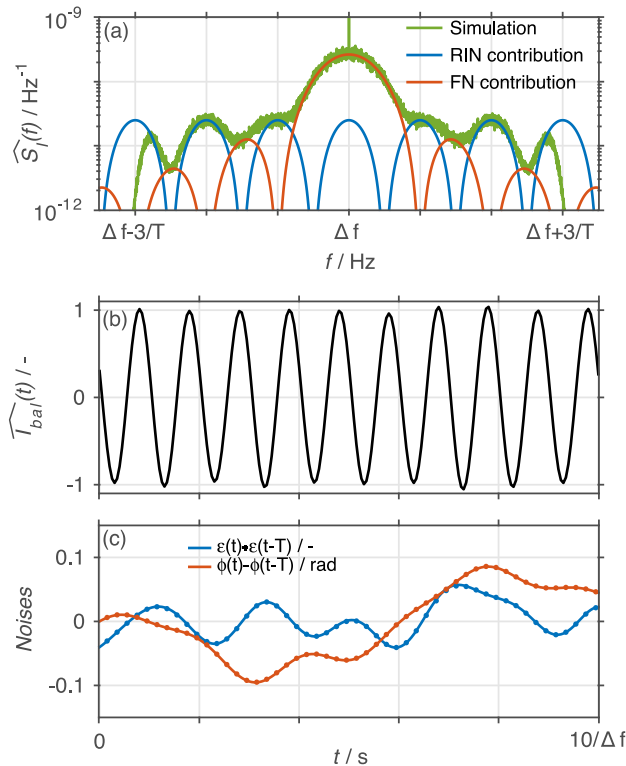
Figure 3. (a) Single-sided normalized photocurrent PSD of the coherent discriminator using an AOM as an active device. The simulation parameters are identical to those of figure 2(a), but the amplitude noise and phase noise have been bandlimited at $3/T$ to avoid aliasing. This signal is more immune to low-frequency additive noise and it does not depend upon the average fringe phase, but it is affected by the RIN in spite of the balancing. (b) Time section of the digitized photocurrent. (c) Noises extracted through signal processing (points) overlaid on the simulation input (solid line). From these two signals, one can independently compute the filtered RIN PSD and FN PSD.

2.3. Simultaneous FN and RIN measurements using the phase diversity approach

We show here that a fully passive design can also solve the problems of the basic coherent discriminator by allowing phase demodulation. In the proposed configuration [figure 1(b)], the output 50/50 coupler is replaced with a 2x4 optical 90° hybrid coupler followed by two balanced photodiodes. Together, these components allow the use of the phase diversity technique used extensively in coherent optical communications [37]. Although the same setup has been demonstrated before, it was only used with interferometer fields decorrelated by multi-kilometer delay-lines [20, 21] and to stabilize the relatively unstable lasers used for data transmission applications [22]. Here, we highlight the advantages and limitations of this configuration used in the coherent regime with optimal signal processing and demonstrate that it can be used for the challenging

noise characterization of highly-stable lasers.

We first obtain expressions for the photocurrents produced by the two balanced photodetectors:

$$I_I(t) \approx \frac{RP_0}{2}[1 + \epsilon(t) + \epsilon(t - T)]$$
$$\times \cos[\phi(t) - \phi(t - T) + 2\pi\nu_0 T], \quad (6a)$$

$$I_Q(t) \approx \frac{RP_0}{2}[1 + \epsilon(t) + \epsilon(t - T)]$$
$$\times \sin[\phi(t) - \phi(t - T) + 2\pi\nu_0 T]. \quad (6b)$$

The approximation symbol is kept instead of the equality symbol since terms of the form $\epsilon^2(t)$ are still neglected, but the expression is otherwise exact. These two photocurrents define an I-Q circle associated with the analytic representation of the signal (figure 4). By digitizing the in-phase and quadrature signals, one can then independently recover the quantities $[I_I(t)^2 + I_Q(t)^2]^{1/2}/I_0 = 1 + \epsilon(t) + \epsilon(t - T) \equiv \alpha(t)$ and $[I_Q(t)/I_I(t)] = \tan[\phi(t) - \phi(t-T) + 2\pi\nu_0 T] \equiv \tan[\psi(t)]$. This replicates all the advantages of performing signal processing on the AOM signal, except for the increased low-frequency additive noise immunity. However, here the extraction operations do not require any assumption about the spectral extent of the noise input, thus overcoming one important limitation of the AOM approach and allowing much more robust processing. This is a substantive advantage for the characterization of stable semiconductor lasers since they can have RIN and FN with bandwidths up into the gigahertz range [38]; the AOM shift required to allow complex filtering is then extreme or even beyond the current technological limit of ∼1 GHz for a single device, or some stringent optical filtering has to be performed before the photodetection step to guarantee that the noise bandwidth is below Δf.

From figure 4, it is obvious that the correct phase and amplitude information cannot be properly extracted without knowledge of the two DC values: AC-coupled detection would bring the noise trace to the center of the I-Q plane, provided the standard deviation of the phase difference is much below one radian as it should be for coherent operation, and this would prevent the proper use of the arctangent operation. This is a disadvantage with respect to the AOM extraction that can work with AC-coupled detectors. However, this limitation highlights a very important advantage of the phase diversity approach: AC-coupled detection is still possible if the DC offsets are measured separately, for example with slow monitor outputs, and restituted during signal processing. Therefore, the full dynamic range of the AC-coupled detector can be used to measure the noise terms. This dynamic range optimization is not possible with the AOM extraction because of the large signal swings at the shifting frequency Δf [figure 3(b)]. This point is crucial for the characterization of highly-
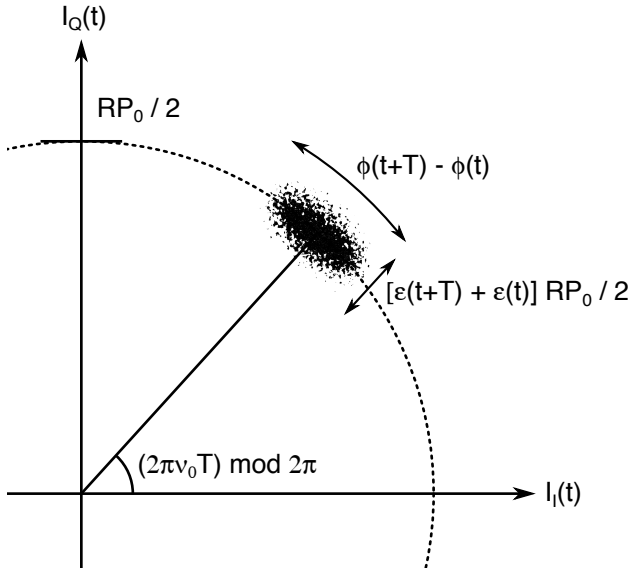
Figure 4. Simple representation of the I-Q circle and the graphical relation between the introduced variables. Phase noise and amplitude noise can be properly extracted only when this circle is perfect.

stable lasers that display extremely small amplitude and phase noises.

Once the terms $\alpha(t)$ and $\psi(t)$ are extracted from the two data streams, one can perform the Fourier transform of the AC autocorrelation functions of these terms, $R(\tau)$, where τ is the lag, in order to compute the relevant power spectral densities. This yields

$$\mathcal{F}\left[R_\psi(\tau)\right] = 4\sin^2(\pi fT)S_\phi(f)$$
$$= (2\pi T)^2\mathrm{sinc}^2(fT)S_\nu(f), \qquad (7a)$$
$$\mathcal{F}\left[R_\alpha(\tau)\right] = 4\cos^2(\pi fT)S_\epsilon(f)$$
$$= \cos^2(\pi fT)S_{\mathrm{RIN}}(f), \qquad (7b)$$

where one once again recognizes the transfer function of a delayed sum, $4\cos^2(\pi fT)$, and delayed difference, $4\sin^2(\pi fT)$. Within the bandwidth of these transfer functions, we also see that the FN PSD and RIN PSD are recovered without ambiguity if the value of the delay T is known with sufficient accuracy. Finally, from the amplitude-phase cross-PSD, one can compute the spectral coherence function $\gamma_{\epsilon,\phi}(f)$. This function is equal to 1 when amplitude and phase are perfectly correlated, and it takes the value 0 when they are fully decorrelated [31]:

$$\left|\mathcal{F}\left[R_{\alpha,\psi}(\tau)\right]\right| = \left|2\sin(2\pi fT)S_{\epsilon,\phi}(f)\right|$$
$$= \sqrt{\mathcal{F}\left[R_\alpha(\tau)\right]\mathcal{F}\left[R_\psi(\tau)\right]}\gamma_{\epsilon,\phi}(f). \qquad (8)$$

Finally, it is important to mention that the configuration of figure 1(b) relies on the assumption of an exact 90° phase shift from the hybrid coupler and equal channel gains to extract two useful signals. In practice, phase and gain imbalances cause an effective distortion of the I-Q plane [39] that can be corrected, as we will show, using schemes commonly used in digital quadrature-amplitude modulation receivers [40]. Typical optical 90° hybrids coupler can have a wavelength-dependent phase imbalance of a few degrees, and omitting the straightforward correction introduces a spurious cross-contamination between phase and amplitude noises. Unequal downstream filtering of the two channels, either in amplitude or in phase, also introduces undesirable distortion. In conclusion, the phase diversity approach appears competitive with the AOM approach when the signal is digitized to allow phase extraction, with clear advantages in terms of bandwidth and dynamic range but a lesser immunity to typical additive noise whose power rises at low frequencies. In practice, the preferable approach depends on the expected additive noise properties, the anticipated laser noise levels and bandwidths, the performance of the optical components, and the overall cost.

3. Experimental demonstration

3.1. Setup and equipment

We perform a proof-of-principle experiment by measuring the noise of a highly-stable single-frequency fiber laser at 192 THz (1560 nm) (NKT, Koheras BoostiK E15). In order to diminish its low-Fourier-frequency FN and show that the phase diversity technique works well even in the most challenging conditions, the laser frequency is actively stabilized to an Ultra Low Expansion glass cavity using the Pound-Drever-Hall (PDH) technique [41]. The generated error signal is scaled and filtered by a proportional-integral (PI) lockbox (New Focus, LB1005) and fed back to a slow piezoelectric actuator inside the laser cavity, yielding 60 mW of stabilized laser power available for characterization, a quarter of which reaches each photodiode in the absence of significant optical loss.

The interferometer of figure 1(b) is built using a PM 50/50 coupler, 100 meters of PM fiber as the delay-line, and a 2x4 90° hybrid coupler (Kylia, COH24). PM fiber is used here for a simple interfacing with our 90° hybrid coupler that requires linearly polarized input signals, but it is not mandatory in general. For this configuration, stimulated Brillouin scattering, which is the first nonlinear effect that could distort the measurement, has a computed threshold that is roughly 10 times higher than the optical power in the delay arm [42]. Furthermore, the delay of 480 ns is more than two orders of magnitude below the coherence time of the free-running laser (75 μs at $1/e$, for a measurement time of 1 s) and more than three order of magnitude below the coherence time of the cavity-locked laser (900 μs). This arm length

imbalance generates a first null at 2.06 MHz in the FN PSD and 1.03 MHz in the RIN PSD; this allows for a proper characterization of the laser noise up to the relaxation oscillations, which here sit at roughly 200 kHz as was specified by the manufacturer.

As stated before, in any interferometric phase measurement the interferometer becomes the implicit reference for the measured noise, just like the LO laser is in an heterodyne measurement. The value of the differential delay T is therefore passively stabilized by tightly wrapping the fiber on a polished granite cylinder. This cylinder is held in an hermetically-sealed box built with acrylic and vibration damping sheets and it sits on an active vibration isolation table (TableStable, TS-300 LP). The entire setup is kept in an acoustic enclosure (Herzan, The Crypt). By incrementally testing the system with increasing acoustic and thermal shielding, we have established that such level of passive stabilization is necessary to properly characterize this specific laser.

The four optical outputs of the 90° hybrid coupler each provide a signal having a power of approximately 13 mW. These signals are measured with DC-coupled balanced InGaAs photodiodes (Discovery Semiconductors, DSC710) having a bandwidth of 10 GHz, a responsivity of 0.75 A/W at 194 THz (1550 nm), and a 50 Ω internal conversion resistor. The electrical signals are low-pass filtered to avoid aliasing and then digitized using a RedPitaya V1.1 board. At our sampling rate of 3.91 MHz, the two input channels each provide a nominal 14-bit vertical resolution. At this bit depth, the white noise floor due to quantization is roughly 10^{-15} V^2/Hz, translating to 10^{-4} Hz^2/Hz white FN PSD. This is significantly better than the standard 8-bit vertical resolution (10^{-12} V^2/Hz) provided by most commercially available oscilloscope, thus enabling a safer use of DC-coupled detectors.

3.2. Signal processing

The two digitized signals are first corrected to account for the imperfect phase shift of the hybrid coupler (0.45°) as well as the gain imbalance of the detection channels (70%). This is achieved by temporarily modulating the laser frequency to completely explore the I-Q ellipse (figure 5). Both corrected signals are then sliced into multiple segments of 300 ms and the phase and amplitude are extracted as explained in section 2.3. For each segment, a second-order polynomial fit is performed on the extracted phase in order to remove the effect of a slow thermally-induced drift of the fringe phase $2\pi\nu_0 T$. This procedure also removes real low-frequency FN information and is not strictly necessary, but it simplifies the rest of the signal processing as was explained with a
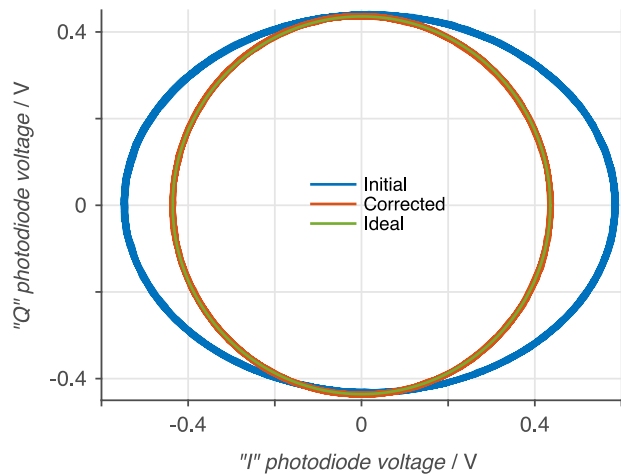

Figure 5. Imperfections of the optical and electrical components lead to a distorted I-Q plane. Signal processing is required to rectify this plane before the signal extraction. In the displayed experimental data, the amplitude imbalance is large but the phase error is modest and not noticeable by eye. There is also a significant DC offset.

different procedure in [11]. A quadratic fit is also performed on the extracted amplitude to account for a slow laser power drift. From the corrected phase and amplitude signals, the amplitude-phase spectral coherence function is finally obtained. The Hann apodization window is applied on all signals and the three modified periodograms are computed using a fast Fourier transform (FFT) algorithm. The spectral shape of the periodograms is then flattened through division by the theoretical functions [using (7a), (7b), and (8)]. This is only done between DC and a fraction of the first null frequency to avoid division by zero.

3.3. Results and discussion

Applying this signal processing routine on a 40-second data stream provides the single-sided (SS) FN PSD from 10 Hz to 1 MHz for the free-running laser and the cavity-locked laser (figure 6, blue and red curves). In each case, the displayed spectrum results from the average of 140 spectra. The frequency axis starts after the points that have been affected by the polynomial fit included in our analysis. The free-running laser's FN PSD [blue, (i)] is in general agreement with the datasheet provided by the manufacturer except for the sharp peaks that are presumably pickup of various electronic and acoustic noises present in our laboratory. These peaks are also visible in other offline heterodyne measurements (not shown here), suggesting that this pickup is not a characteristic of the interferometer but of the laser itself.

The FN PSD of the cavity-locked laser [red, (ii)] displays a characteristic servo hump around 10
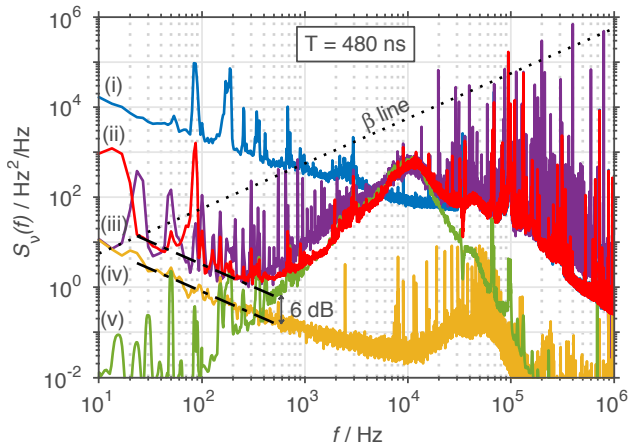
Figure 6. Single-sided frequency noise PSD extracted from a 480-ns-delay passive coherent discriminator compared with a number of measurements that verify our results. (i) Free-running laser noise (blue). (ii) Cavity-locked laser noise (red). (iii) Heterodyne measurement with a second highly-stable laser (purple). (iv) Additive noise that is measured in the absence of light, offset at the proper I-Q radius, and converted to FN (yellow). (v) Error signal input to the 10-kHz bandwidth PI filter converted to FN (green, not valid above 10 kHz). The β-separation line [6] is also plotted.

kHz. However, low-Fourier-frequency noise does not follow the ideal $1/f^2$ spectral power suppression that should be provided by the locking system, which in this region is that of a pure integrator. Still, the correct setting of the locking system is confirmed by observing the residual in-loop signal of the PDH lock [green, (v)]: this curve displays the anticipated attenuation relative to the unlocked laser's FN PSD. This suggests that some noise is introduced before the PI filter, most likely delivery fiber flicker noise, and prevents a proper suppression at low frequencies. To gain more information, we performed an heterodyne measurement with the best available reference in our laboratory: a second highly-stable laser with similar performances. The purple (iii) curve of figure 6 is the spectrum obtained from this measurement after performing signal processing equivalent to that performed on the interferometer data.

From the comparison of the red (ii) and purple (iii) curves, we make two observations. The first one is that the heterodyne measurement does not provide reliable information between 1 and 10 kHz since this region is obviously slightly degraded by the "reference" laser's FN. We conclude this since the measurement with the interferometer exactly reproduces the scaled error signal [green, (v)]. We can thus establish that, at least for this Fourier frequency region, the interferometer allows us to make remarkably low frequency noise measurements without the need for an additional high quality laser. Indeed, in this case the performance of our second laser was insufficient to resolve the actual

noise of the cavity-locked laser. The second observation is that the floors of the interferometer measurement and the heterodyne measurement approximately agree below 300 Hz except for a number of peaks: the peaks between 200 Hz and 1 kHz were observed in other measurements (not shown here) of the reference laser and thus belong to it; the sharp peak at 90 Hz and the hump at 15 Hz, however, are presumed to arise from acoustic perturbations of the interferometer. We therefore conclude that, except for these two presumably-acoustic features, the interferometer is measuring laser noise even for the lowest displayed Fourier frequencies.

Even with careful improvement of the stabilization system so that the cavity-locked laser FN [red, (ii)] better follows the ideal $1/f^2$ spectral power suppression [green, (v)], the additive noise [yellow, (iv)] sits only $\approx$ 6 dB below the currently measured frequency noise level between 10 Hz and 300 Hz. For any significant diminution of this level, the additive noise will become the dominant measurement floor in this Fourier frequency region. In our case, this additive noise originates from the digitizer board and is not due to quantization. It was obtained by measuring the electrical signal in the absence of light at different stages in the detection chain and then converting the dominant signal to an equivalent FN PSD for analysis purposes [43]. Since there is no optical signal in this verification measurement, the DC offsets and the fringe phase have to be manually added to the digitized noise signals to allow for a proper conversion (see figure 4). Here we set the same I-Q radius as in figure 5 and $2\pi\nu_0 T = 0$, which means that the additive noise in one channel of the digitizer board is directly converted to phase noise, while the additive noise in the second channel is directly converted to amplitude noise. This additive noise floor was an anticipated limit, but there is still place for improvement as a higher optical power or low-noise acquisition electronics can be used to push down its onset. Morever, since the additive noise is not coming from the detector but from the digitizer board, this limit could be significantly lowered through the electrical amplification of AC-coupled signals before digitization, provided of course that the DC-levels are measured in parallel and restituted during signal processing. We finally note that with this level of additive noise and under the current experimental conditions, a standard 8-bit digitizer would have been sufficient instead of a 14-bit digitizer.

The signal processing also provides the SS RIN PSD from 10 Hz to 1 MHz [figure 7(a)]. We observe that there is almost no dependence of this quantity on the locking condition. This is to be expected as the RIN should not appreciably vary with small changes in the laser cavity length produced by driving a well-
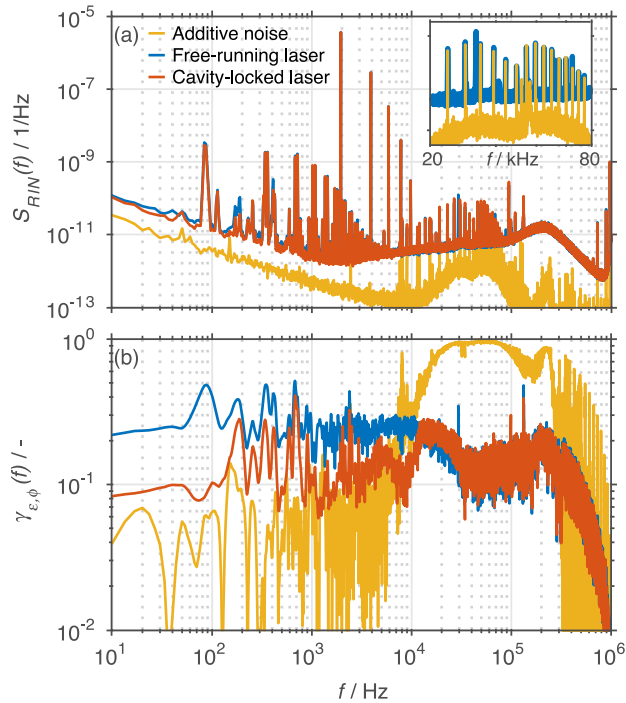
Figure 7. (a) Single-sided relative intensity noise PSD. The smooth hump at 200 kHz correspond to the relaxation oscillations frequency. The inset shows the details between 20 and 80 kHz. (b) Amplitude-phase spectral coherence function (smoothed). In both cases, the locked and unlocked signals are compared with the signal obtained by applying the same signal processing on properly offset additive noise.

aligned piezoelectric actuator [44]. These two traces are also in agreement with an independent direct RIN measurement (i.e. using the conventional method) taken with the same digitizer board and same signal level, not shown here to avoid overloading the plot. From the comparison with the equivalent RIN PSD produced by additive noise, it is however obvious that there is some contamination by sharp additive noise peaks between 10 and 100 kHz; the peaks of the yellow trace match those of the interferometric measurements in position, width, and height, as is more clearly shown in the inset. Moreover, the RIN PSD is barely above the noise floor below 2 kHz. This noise floor could be lowered by applying the solutions that we earlier suggested for the FN measurement.

The second panel of figure 7 shows the SS spectral coherence function $\gamma_{\epsilon,\phi}(f)$ that was here smoothed with a 6-point moving average (equivalent to 20 Hz) to highlight the general trend. In this plot, we observe a modest decrease in amplitude-phase correlation within the servo bandwidth (<10 kHz). This is also to be expected as the amplitude noise does not change appreciably when a piezoelectric actuator is used, whereas phase noise is diminished by locking the laser to a stable reference cavity: this reduces the

initial correlation that originates from the dynamics of the laser [45]. In the same plot, we show in yellow the spectral coherence function, which in this case characterizes the correlation between the additive noises of the two acquisition channels. This is true only because $2\pi\nu_0 T = 0$ was used during the signal processing, guaranteeing that the two signals are not artificially mixed together. Between 10 and 100 kHz, we see that the two additive noise signals are almost perfectly correlated. This suggests that the additive noise in this frequency range is coming from the digitizer board itself and not from the individual front-ends. This undesirable property could be caused by spurious coupling of the clock signal or insufficient power supply decoupling on the RedPitaya board.

4. Conclusion

We have presented an entirely passive coherent discriminator that uses an optical 90° hybrid coupler to perform in-phase and quadrature detection of laser noise. Like other conventional coherent discriminators, this technique permits the measurement of laser FN without requiring a second, more stable reference laser or an inconveniently long optical delay-line. We have performed a comparative theoretical analysis showing that this technique solves the main problems of the basic coherent discriminator by allowing phase demodulation of the digitized output signal in a way similar to the coherent self-heterodyne technique. Contrary to this conventional improvement of the basic coherent discriminator that is based on an AOM, the phase diversity approach provides a robust phase extraction under all experimental conditions, a potential optimal use of the detection dynamic range, and a fully passive hardware setup. These qualities make it interesting as a general testbed for research and industry, as an instrument that can be more easily carried in the field, or as an ultimate reference for highly-stable lasers when a second more stable oscillator is not available. In this last case, the stabilization of the delay-line still has to be performed with great care as it becomes the new implicit phase reference. We have also highlighted the limitations of the technique, namely the necessity to measure the DC offsets, the need to account for the imperfect 90° hybrid coupler through calibration, and the susceptibility to low-frequency additive noise contamination. This last point has been specifically illustrated in the experimental demonstration of the instrument, in which the laser's relative intensity noise and the amplitude-phase spectral coherence function were simultaneously extracted. This demonstration should be relevant for all scientists and engineers performing laser noise characterization.

Acknowledgments

Appendix: Comments on the Choice of Correlation Regime

We want to point out that (2), (5), (6a), and (6b) [but not (3)] are valid regardless of the value of T (coherent or incoherent regime), provided that we keep the two assumptions made before the introduction of (2). In section 2, we have focused on cases for which the standard deviation of the differential phase is small (coherent regime), allowing a linearization of the cosine function as in (3), even though we have also presented two techniques where the differential phase is instead exactly extracted through signal processing. Alternatively, in the incoherent regime the combined fields are decorrelated and the standard deviation of the differential phase becomes much larger than 2π; the output cannot be linearized. If no more signal processing is performed on the digitized data, for example when a spectrum analyzer is directly used to characterize the photocurrent produced by the incoherent interferometer, the computed noise spectrum is then the self-convolution of the initial laser lineshape. This spectrum is similar to the initial laser lineshape (since the phase noise is still inside a cosine function), albeit with twice the phase noise power, and centered at DC or at the AOM shifting frequency (for example, the incoherent homodyne interferometer for (2) [12], and the incoherent self-heterodyne interferometer for (5) [28]). Information about the initial laser lineshape can therefore be obtained from this photocurrent PSD.

However, we insist this does not mean that the incoherent interferometer can only provide lineshape measurements; the differential phase noise can just as well be extracted from digitized data if an AOM or a 90° hybrid coupler is properly used as was done in section 2.3 for the coherent case. From this recovered signal, one can still compute the FN PSD. Another way to see this is to recognize that the phase difference produced by the interferometer
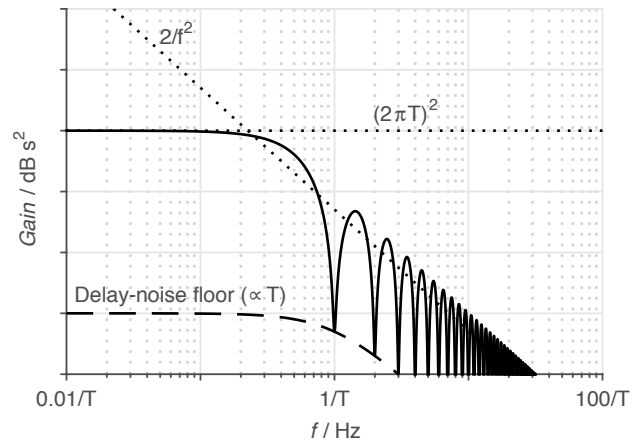

Figure A1. General tranfer function applied to the FN PSD for any two-beam interferometer configuration relying on phase extraction or demodulation (valid for any coherence regime). The delay T can be freely adjusted so that the noise of interest sits before $f = 1/T$, in the approximately flat section of the transfer function where the SNR scales with T.

leads to a FN PSD multiplied by a squared cardinal sine function regardless of the value of T. For a short delay, the relevant laser noise can be kept before the first null of the transfer function; it is then desirable for the measurement time to be much longer than the interferometer delay in order to measure the PSD over a significant Fourier frequency range below $1/T$ (figure A1). For a long delay, the relevant noise can instead be kept outside of the first lobe. In this case it is typically better for the measurement time to be much shorter than the interferometer delay; the resolution bandwidth is then insufficient to resolve the oscillation of the transfer function, and the average gain of $2/f^2$ is effectively applied; this is twice the conversion factor between the phase noise PSD and frequency noise PSD. Hence, when the differential phase is extracted and processed instead of its cosine, a short delay with a much longer measurement time produce a flat transfer function for frequency noise, whereas a long delay with a much shorter measurement time produce a flat transfer function for phase noise.

The important conclusion is that the same spectral information can be theoretically extracted with both the coherent and incoherent versions of the interferometer if a phase extraction or demodulation is performed. This stems from the fact that demodulation replaces linearization and is valid regardless of the standard deviation of the differential phase noise. In a sense, the regime of coherence thus becomes irrelevant and the interferometer delay can be freely chosen based on practical matters. For the characterization of highly-stable lasers, this motivates the use of relatively short delays for several reasons. First, and as stated before, stable lasers

have electric field autocorrelation functions that show a very slow decay (high temporal coherence) and trying to operate in the incoherent regime often forces the use of impractically long delay-lines. Second, longer fiber delays lead to an increase in optical nonlinearities and differential absorption, which are both sources of instrumental errors or noises. This last point is especially important for the characterization of highly-stable lasers emitting in a spectral range of poor optical fiber transparency, such as some mid-infrared lasers [46].

Finally, the fringe phase $2\pi\nu_0 T$ is in *all cases* added to the extracted phase term. The value of T has been assumed constant in most of the previous theoretical treatment, but in practice it is a stochastic value because of acoustic and thermal fluctuations. It therefore contributes to the measured FN PSD and potentially contaminates it. Taking it into account, the real extracted noise is:

$$\mathcal{F}[R_\psi(\tau)] \approx (2\pi T)^2 \text{sinc}^2(fT)S_\nu(f) + (2\pi\nu_0)^2 S_T(f) \tag{A.1}$$

where $S_T(f)$ is the delay noise PSD $[(2\pi\nu_0)^2 S_T(f)$ is then the fringe phase noise PSD introduced by the delay-line]. For typical noise environments and passive stabilization capabilities, the delay noise PSD has a low-pass spectral shape that only rises with longer delay [47], but it most often increases linearly instead of quadratically with T because of the low spatial correlation of the noise [48] (figure A1). To minimize the effect of delay noise when phase extraction is performed, the correct procedure is then to set the delay so that the noise of interest completely fits within the first lobe of the transfer function illustrated in figure A1 (below $f = 1/T$). In other words, the instrument bandwidth, proportional to $1/T$, and the measured noise bandwidth must be matched. In this Fourier frequency region only, increasing the delay also increases the measurement gain and the ratio between FN, which is to be measured, and delay noise, which is a source of contamination. If this matching condition is not respected, the noise of interest must at least partially sit in the Fourier frequency region where the gain averages to $2/f^2$; further increasing the delay in this case only leads to a higher proportion of delay noise in (A.1), an undesirable effect. The same argument can be made for interferometers that do not rely on phase extraction and operate in the incoherent regime: the gain on the signal is fixed while the delay noise increases with T. Thus, taking all the mentioned effects into account, there appears to be no advantage in working with incoherent or long-delay interferometers for the noise characterization of highly-stable lasers.

References

[1] Svelto O and Hanna D C 2010 *Principles of lasers* (Springer)
[2] Ludlow A D, Boyd M M, Ye J, Peik E and Schmidt P O 2015 *Rev. Mod. Phys.* **87** 637 URL http://journals.aps.org/rmp/abstract/10.1103/RevModPhys.87.637
[3] Ip E, Lau A P T, Barros D J and Kahn J M 2008 *Opt. Lett.* **16** 753–791 URL https://www.osapublishing.org/oe/abstract.cfm?uri=oe-16-2-753
[4] Demtröder W 2013 *Laser spectroscopy: basic concepts and instrumentation* (Springer)
[5] Riehle F 2006 *Frequency standards: basics and applications* (John Wiley & Sons)
[6] Di Domenico G, Schilt S and Thomann P 2010 *Appl. Opt.* **49** 4801–4807 URL https://www.osapublishing.org/ao/abstract.cfm?uri=ao-49-25-4801
[7] Egan W F 1988 *IEEE Trans. Instrum. Meas.* **37** 240–244 URL http://ieeexplore.ieee.org/xpls/abs_all.jsp?arnumber=6059
[8] Cummins H Z 2013 *Photon correlation and light beating spectroscopy* vol 3 (Springer)
[9] Kessler T, Hagemann C, Grebing C, Legero T, Sterr U, Riehle F, Martin M, Chen L and Ye J 2012 *Nature Photon.* **6** 687–692 URL http://www.nature.com/nphoton/journal/v6/n10/abs/nphoton.2012.217.html
[10] Bernier M, Michaud-Belleau V, Levasseur S, Fortin V, Genest J and Vallée R 2015 *Optics letters* **40** 81–84 URL https://www.osapublishing.org/ol/abstract.cfm?uri=ol-40-1-81
[11] Schiemangk M, Spießberger S, Wicht A, Erbert G, Tränkle G and Peters A 2014 *Appl. Opt.* **53** 7138–7143 URL https://www.osapublishing.org/ao/abstract.cfm?uri=ao-53-30-7138
[12] Nazarathy M, Sorin W V, Baney D M, Newton S *et al.* 1989 *J. Lightwave Technol.* **7** 1083–1096 URL http://ieeexplore.ieee.org/xpls/abs_all.jsp?arnumber=29635
[13] Armstrong J 1966 *J. Opt. Soc. Am. A* **56** 1024–1028 URL https://www.osapublishing.org/josa/abstract.cfm?uri=josa-56-8-1024
[14] Moslehi B 1986 *J. Lightwave Technol.* **4** 1704–1710 URL http://ieeexplore.ieee.org/xpls/abs_all.jsp?arnumber=1074674
[15] Lance A L, Seal W D and Labaar F 1984 *Int. J. Infrared Millim. Waves* **11** 239–289 URL http://tf.nist.gov/general/tn1337/Tn190.pdf
[16] Sorin W V, Chang K W, Conrad G and Hernday P R 1992 *J. Lightwave Technol.* **10** 787–793 URL http://ieeexplore.ieee.org/xpls/abs_all.jsp?arnumber=143079
[17] Turcotte C S, Tremblay P and Genest J 1998 Semiconductor lasers used as the metrology source in Fourier-transform spectrometers: effect of their noise *Proc. SPIE 3415* pp 122–134 URL http://proceedings.spiedigitallibrary.org/proceeding.aspx?articleid=954611
[18] Tur M, Moslehi B, Bowers J, Newton S, Jackson K, Goodman J, Cutler C and Shaw H 1983 Spectral structure of phase-induced intensity noise in recirculating delay lines *Proc. SPIE 0412* pp 22–27 URL http://proceedings.spiedigitallibrary.org/proceeding.aspx?articleid=1235623
[19] Tremblay P and Ouellet R 1991 *IEEE Trans. Instrum. Meas.* **40** 204–207 URL http://ieeexplore.ieee.org/xpls/abs_all.jsp?arnumber=1032916
[20] Shi K, Watts R, Reid D, Huynh T N, Browning C, Anandarajah P M, Smyth F and Barry L P 2011 *IEEE Photon. Technol. Lett.* **23** 1591–1593 URL http://ieeexplore.ieee.org/xpls/abs_all.jsp?

arnumber=5983399

[21] Huynh T N, Nguyen L and Barry L P 2013 *J. Lightwave Technol.* **31** 1300–1308 URL https://www.osapublishing.org/jlt/abstract.cfm?uri=jlt-31-8-1300

[22] Lavery D, Maher R, Paskov M, Thomsen B C, Bayvel P and Savory S J 2013 *IEEE Photon. Technol. Lett.* **25** 2213–2216 URL http://ieeexplore.ieee.org/xpl/login.jsp?tp=&arnumber=6612652&url=http%3A%2F%2Fieeexplore.ieee.org%2Fxpls%2Fabs_all.jsp%3Farnumber%3D6612652

[23] Barnes J 1966 *Proc. IEEE* **54** 207–220 URL http://ieeexplore.ieee.org/xpls/abs_all.jsp?arnumber=1446563

[24] Suhara T 2004 *Semiconductor laser fundamentals* (CRC Press)

[25] Meng Z, Hu Y, Xiong S, Stewart G, Whitenett G and Culshaw B 2005 *Appl. Opt.* **44** 3425–3428 URL https://www.osapublishing.org/ao/abstract.cfm?uri=ao-44-17-3425

[26] Santis C T, Steger S T, Vilenchik Y, Vasilyev A and Yariv A 2014 *Proc. Natl. Acad. Sci. U.S.A.* **111** 2879–2884 URL http://www.pnas.org/content/111/8/2879.short

[27] Goobar E 1993 *IEEE J. Quantum Electron.* **29** 1116–1130 URL http://ieeexplore.ieee.org/xpls/abs_all.jsp?arnumber=214498&tag=1

[28] Okoshi T, Kikuchi K and Nakayama A 1980 *Electron. Lett.* **16** 630–631 URL http://ieeexplore.ieee.org/xpls/abs_all.jsp?arnumber=4244210

[29] Gallion P, Mendieta F and Leconte R 1982 *J. Opt. Soc. Am. A* **72** 1167–1170 URL https://www.osapublishing.org/josa/abstract.cfm?uri=josa-72-9-1167

[30] Ktonas P Y and Papp N 1980 *Signal Process.* **2** 373–385 URL http://www.sciencedirect.com/science/article/pii/0165168480900791

[31] Tsuchida H 1998 *Opt. Lett.* **23** 1686–1688 URL https://www.osapublishing.org/ol/abstract.cfm?uri=ol-23-21-1686

[32] Clubley D, Newton G, Skeldon K, Strain K and Hough J 2001 *J. Opt. A: Pure Appl. Opt.* **3** 196 URL http://iopscience.iop.org/article/10.1088/1464-4258/3/3/308/meta;jsessionid=95F28245FFA8CFFEB16CE56EF9054812.c4.iopscience.cld.iop.org

[33] Tarn C W, Banerjee P P, Liu J J and Pliszka P 1992 Performance of acousto-optic devices in the presence of noise *Proc. SPIE 1844* pp 155–161 URL http://proceedings.spiedigitallibrary.org/proceeding.aspx?articleid=1005020

[34] Coquin G, Pinnow D and Warner A 1971 *J. Appl. Phys.* **42** 2162–2168 URL http://scitation.aip.org/content/aip/journal/jap/42/6/10.1063/1.1660520

[35] Eschler H 1976 *Appl. Phys.* **9** 289–306 URL http://link.springer.com/article/10.1007/BF00900455

[36] Niwa Y, Arai K, Ueda A, Sakagami M, Gouda N, Kobayashi Y, Yamada Y and Yano T 2009 *Appl. Opt.* **48** 6105–6110 URL https://www.osapublishing.org/ao/abstract.cfm?uri=ao-48-32-6105

[37] Hui R and O'Sullivan M 2009 *Fiber optic measurement techniques* (Academic Press)

[38] Numata K, Alalusi M, Stolpner L, Margaritis G, Camp J and Krainak M 2014 *Opt. Lett.* **39** 2101–2104 URL https://www.osapublishing.org/ol/abstract.cfm?uri=ol-39-7-2101

[39] Harris F 1996 Digital filter equalization of analog gain and phase mismatch in IQ receivers *Proc. IEEE Int. Conf. Universal Personal Commun.* vol 2 pp 793–796 URL http://ieeexplore.ieee.org/xpls/abs_all.jsp?arnumber=562684

[40] Tubbax J, Côme B, Van der Perre L, Donnay S, Engels M, De Man H and Moonen M 2005 *IEEE Trans. Wireless Commun.* **4** 872–877 URL http://ieeexplore.ieee.org/xpls/abs_all.jsp?arnumber=1427677

[41] Drever R, Hall J L, Kowalski F, Hough J, Ford G, Munley A and Ward H 1983 *Appl. Phys. B* **31** 97–105 URL http://link.springer.com/article/10.1007/BF00702605

[42] Smith R G 1972 *Appl. Opt.* **11** 2489–2494 URL https://www.osapublishing.org/ao/fulltext.cfm?uri=ao-11-11-2489&id=17442

[43] Tremblay P, Têtu M and Michaud A 1989 *IEEE Trans. Instrum. Meas.* **38** 967–973 URL http://ieeexplore.ieee.org/xpl/login.jsp?tp=&arnumber=39038&url=http%3A%2F%2Fieeexplore.ieee.org%2Fxpls%2Fabs_all.jsp%3Farnumber%3D39038

[44] Cranch G 2002 *Opt. Lett.* **27** 1114–1116 URL https://www.osapublishing.org/ol/abstract.cfm?uri=ol-27-13-1114

[45] Foster S 2007 *IEEE Photon. Technol. Lett* **19** 895–897 URL http://ieeexplore.ieee.org/xpl/login.jsp?tp=&arnumber=4212156&url=http%3A%2F%2Fieeexplore.ieee.org%2Fxpls%2Fabs_all.jsp%3Farnumber%3D4212156

[46] Méndez A and Morse T F 2011 *Specialty optical fibers handbook* (Academic Press)

[47] Stefani F, Lopez O, Bercy A, Lee W K, Chardonnet C, Santarelli G, Pottie P E and Amy-Klein A 2015 *J. Opt. Soc. Am. B* **32** 787–797 URL https://www.osapublishing.org/josab/abstract.cfm?uri=josab-32-5-787

[48] Sheard B S, Gray M B and McClelland D E 2006 *Appl. Opt.* **45** 8491–8499 URL https://www.osapublishing.org/ao/abstract.cfm?uri=ao-45-33-8491